

Learning a Disentangled Embedding for Monocular 3D Shape Retrieval and Pose Estimation

Kyaw Zaw Lin¹ Weipeng Xu² Qianru Sun^{1,2} Christian Theobalt² Tat-Seng Chua¹

¹National University of Singapore

²Max Planck Institute for Informatics, Saarland Informatics Campus

kyawz1@comp.nus.edu.sg {wxu, qsun, theobalt}@mpi-inf.mpg.de

{dcssq, dcscts}@nus.edu.sg

Abstract

We propose a novel approach to jointly perform 3D object retrieval and pose estimation from monocular images. In order to make the method robust to real world scene variations in the images, e.g. texture, lighting and background, we learn an embedding space from 3D data that only includes the relevant information, namely the shape and pose. Our method can then be trained for robustness under real world scene variations without having to render a large training set simulating these variations. Our learned embedding explicitly disentangles a shape vector and a pose vector, which alleviates both pose bias for 3D shape retrieval and categorical bias for pose estimation. Having the learned disentangled embedding, we train a CNN to map the images to the embedding space, and then retrieve the closest 3D shape from the database and estimate the 6D pose of the object using the embedding vectors. Our method achieves 10.8 median error for pose estimation and 0.514 top-1-accuracy for category agnostic 3D object retrieval on the Pascal3D+ dataset. It therefore outperforms the previous state-of-the-art methods on both tasks.

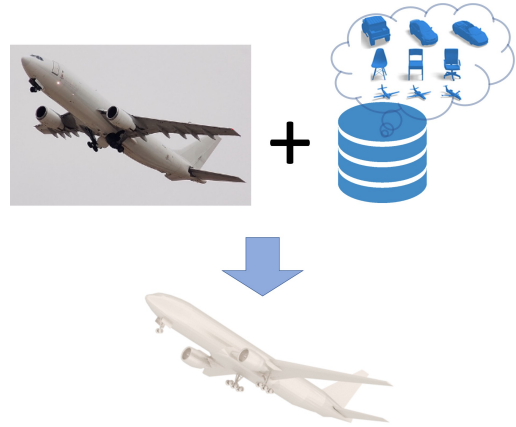


Figure 1. Given a single RGB image of an object, our method retrieves its closest 3D shape from a database and estimates its 6D pose.

1. Introduction

The task of estimating 3D shape and pose from monocular images (see Figure. 1) are highly correlated and under-constrained. Many state-of-the-art approaches phrase it as a retrieval from database and pose estimation. Solving these two problems jointly is an important topic for computer vision, which has a broad range of applications in many areas such as augmented reality, 3D scene understanding and robotics.

In recent literature, many of the existing methods rely on training convolutional neural networks (CNN) using synthetic images rendered with the CAD models [3, 4, 19, 16],

due to the difficulty of collecting large scale annotated training datasets of real images. Many methods learn to match synthetic image features against the real image features to factor out the appearance discrepancy between 3D models and real objects [16, 27, 47]. However, there is a significant gap between real images and rendered images due to distracting factors such as the varying lighting conditions, appearance, camera response functions and backgrounds, which leads to low generalizability of the methods to natural images. Furthermore, the appearance of the objects is also dependent on the poses. Typically, one has to render a large number of images from CAD models with different textures and poses in order to cover the appearance variation. But simulating all possible variations graphically is prohibitive and still leads to limited generalizability.

In order to alleviate this problem, [16] proposes 1) to render depth images instead of RGB images to circumvent the real vs. synthetic domain gap due to texture, lighting and background, and 2) to first estimate the pose of the ob-

ject and only render the 3D models in the estimated pose, which significantly reduces the rendering cost during testing. However, they still have to render the 3D models in densely sampled poses for training, and more importantly, the error in the pose estimation leads to failure in 3D shape retrieval.

In this paper, we propose a novel approach to jointly perform 3D shape retrieval and pose estimation based on learning a disentangled shape and pose embedding. Specifically, our method consists of two stages: In the first stage, we train a CNN to learn an embedding space from 3D data, which only encodes the relevant scene independent information, namely shape and pose, and therefore is free of environment dependent factors. Furthermore, we explicitly disentangle the shape and pose embedding. Specifically, we train the network with 3D volumes of occupancy grids of the objects in different poses and map them to a pair of embedding vectors, i.e. a shape vector and a pose vector. Benefiting from the disentangling, the learned shape embedding is invariant to the pose and the pose embedding is invariant to the shape. In the second stage, we train another CNN to map the 2D image to the embedding vectors, which allows us to retrieve the 3D shape and estimate its 3D pose simultaneously from the image.

Our method possesses the following advantages: 1) Learning the embedding from 3D data instead of images allows us to eliminate the distracting factors such as texture, lighting and background. 2) The disentangled embedding for shape and pose alleviates both the categorical bias for pose estimation and pose bias for shape retrieval. 3) To learn the embedding space, we do not need to generate multi-view rendered training images with pose variations, which is difficult in practice. Instead, our volumetric training samples in different poses are generated efficiently in an online manner.

Our experimental results show that our method outperforms the state-of-the-art methods on the Pascal3D+ dataset [48] on both 3D shape retrieval and pose estimation tasks.

2. Related work

There is a rich literature on image based object retrieval and pose estimation. We will limit the discussion in this section to the topics that are most related to our work: image-based 3D shape retrieval, 3D pose estimation and joint representation learning.

3D Shape Retrieval from 2D Images. Many methods for 3D shape retrieval rely on synthesized images of 3D models to perform matching between images and 3D models [3, 4, 19, 16]. However, it is challenging to perform direct comparison between CNN features of rendered images and real images due to the domain gap. To overcome this, metric learning approaches are usually adopted to bridge the

gap between the two domains [47, 16]. To further bridge the incompatibility between the two domains, [50, 16] opted to use depth based rendering to reduce the difference between two domains.

To circumvent the problem arising from the use of rendered images, many methods have attempted to use the intrinsic representation of 3D models directly instead of rendered images as proxy for 3D models. Li et al. [24] map image features to light field descriptors computed from 3D models. Tasse et al. [41] use the word2vec [14] as an embedding space and map different input modalities such as 3D model, image and sketch drawing to the same space. Girdhar et al. [13] use voxel reconstruction as embedding space but did not consider pose variations.

Our proposed method has several advantages to existing works. We consider fine-grained model level retrieval, unlike [24, 41], where they only consider category level retrieval. We do not require an additional metric learning stage to bridge the domain gap unlike [16]. Additionally, Grabner et al. [16] need to render 3D models in different viewpoints and search against multiple viewpoints as they does not explicitly decouple pose in their representation. Our 3D representation is able to naturally embed both shape and poses in a disentangled way, unlike [24, 13], where they only consider shape information in their embedding.

3D Shape Representation for 3D Shape Retrieval The existing 3D shape retrieval methods can also be categorized into two groups depending on how to represent 3D models: image-based methods and 3D model based methods. Image based methods learn shape features based on multi-view projection of 3D models [5, 39] and represent 3D models as a set of 2D images. Shi et al. [37] propose a variation on this theme where, instead of multi-view images, a cylinder projection around the object’s principle axis is used to represent 3D object. 3D model based methods [44, 28, 36] directly utilize 3D representations and use 3D CNNs to perform various tasks. Image based methods used to outperform 3D model based methods in terms of retrieval accuracy on large scale 3D shape retrieval dataset [6, 34]. Recently, however, 3D model based methods have started to reach performance parity against image-based methods [7, 36]. In our approach, we make use of the 3D volumetric representation because it is more efficient to perform transformations on voxels than to produce multi-view renderings for arbitrary poses.

3D Pose Estimation. There are two main categories of approaches to 3D pose estimation from 2D images. The first category is based on keypoints detection. These approaches assume that the 3D model of the object is available and predicts 2D keypoints with known correspondences on the 3D model. Then perspective-n-point problem (PnP) is solved to find the transformation parameters, which minimizes distance from 2D projection of 3D points to detected 2D key-

points.

These approaches are commonly used on the specific object classes with limited variations across object instances, for example, on faces [20, 22, 49]. To apply these approaches to general objects, the objects are typically approximated by their 3D bounding boxes and the 8 or 9 points of the enclosing cubes are predicted. In [16], this approach is used to estimate pose, which is later used to render the depth image for retrieval. However, this method has to learn the dimension of the box in addition to the keypoints.

The second category of approaches directly predicts the transformation parameters. Su et al. [43] represent rotations as bins in Euler angles and formulate pose estimation as a classification problem. However, the quantization of angles introduce inaccuracy, even though the classification predictions are accurate. Su et al. [40] address the task using a geometry aware soft weighted classification scheme. Mahendran et al. [25] attempt to improve on it by treating it as a regression problem, which is a more natural formulation of the task. They represent rotations in axis-angle or quaternion space and use geodesic distance as an alternative to L2 distance. However, their method cannot outperform the classification approach in [40].

Recently, hybrid approaches based on classification followed by residual regression [32, 17, 33] have become popular for a variety of different tasks. Such approaches have been applied to pose estimation to achieve state-of-the-art performance on Pascal3D+ dataset [26, 23]. We adopt this hybrid strategy in our framework for pose estimation since it is generic to all objects. Comparing to existing methods, our approach achieves additional robustness afforded by the guidance from the “pure” information learned from 3D data, which is free from distracting factors in the images.

Joint Representation Learning. The idea of using a common and meaningful embedding space has a rich history. A well known example is the word2vec embedding [14] or the more recent GloVe [31], where textual input is embedded in space in which words that share the same context is located close to each other. Using this embedding space, joint image-to-text embeddings [15, 12] have been proposed where images and text can be compared directly, facilitating text to image retrieval or vice versa. An important application of such embeddings has been seen in zero-shot learning [12, 1, 2, 46]. A fixed embedding space based on a language prior also facilitates tasks such as image description [21], where textual descriptions are generated from images.

Following the same idea, common embedding space for shape was proposed in [41], where multiple modalities (3D mesh, image, text etc.) are embedded using the word2vec semantic space. This allows cross-modal retrieval between arbitrary modalities. Different input modalities for embeddings were investigated such as shapes and text [9], shapes and images [45], and sketches and 3D shapes [10]. In our

proposed method, we learn a task specific embedding space shared by images and 3D shapes, which encodes the shape and pose information in a disentangled way.

3. Method

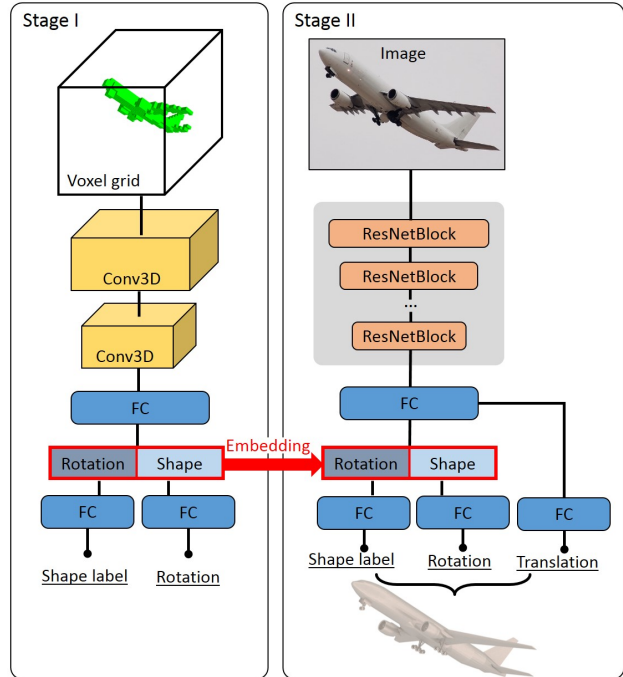


Figure 2. Our method consists of two stages: In the first stage, we learn disentangled embedding space from 3D data, which is free of distracting factors. Then, we train a CNN to map the 2D images to the embedding vectors, which allows us to retrieve the 3D shape and estimate the pose simultaneously for the images.

As shown in Figure 2, our method consists of two stages. In the first stage, we train a CNN (referred as *embedding network*) to learn a disentangled embedding space for shape and pose. In the second stage, we train another CNN (referred as *regression network*) to map a monocular 2D image to the embedding vector, which allows us to retrieve the 3D shape and estimate the 3D pose simultaneously from the images.

3.1. Disentangled Shape and Pose Embedding

To recognize 3D objects from 2D images is a challenging task, since there are many distracting variations in the images, such as textures of the objects, lighting conditions, camera response functions and backgrounds. To alleviate this problem, we learn a discriminative embedding representation of 3D objects that aims to factor out the distracting variations. The learned embedding should only consist of the information that we are interested in, namely, shape and pose. Furthermore, we explicitly disentangle the embedding representation to a shape embedding vector and a

pose embedding vector. On the one hand, this makes the shape recognizer agnostic to the pose and therefore makes it generalize better to objects in unseen poses. On the other hand, this also alleviates the categorical bias in pose estimation.

3.2. Learning the Embedding from 3D Data (Stage I)

Our disentangled shape and pose embedding is illustrated in Figure 2 **Stage I**. Our embedding learning idea is inspired by [24], where the 3D shapes and images are mapped to the “light field” descriptors measuring the similarity of the 3D shapes. However, their representation is not suitable for our purpose, since the pose information is not encoded in their representation. In contrast, our goal is to jointly recognize the shape and estimate its 3D pose. Therefore, we use the 3D volumetric occupancy grid, which is a natural representation for 3D objects, as the input, and learn a pure shape and pose embedding from it. The input 3D volumetric occupancy grid is generated with the *binvox* [29] tool using the CAD models of the objects. The resolution of the input volume is $32 \times 32 \times 32$. We map the input volume to the concatenated embedding vectors of shape and pose using an architecture similar to *VoxNet* [28], which consists of two 3D convolution layers and one fully connected layer.

For training the shape embedding, we impose a cross entropy loss for shape classification. Note that the cross entropy loss can be replaced with a pair-wise distance metric such as triplet ranking loss [35], when dealing with a dataset that consists of a large amount of objects, e.g. the ObjectNet3D dataset [47]. In our experiments, we use the Pascal3D+ dataset [48] that contains 79 objects, where the cross entropy loss is more efficient for training.

In order to learn the pose embedding, we apply random rotations on the 3D volumes during training. Note that the translation is not encoded in the pose embedding, since we observe that the translation is dependent on the image cropping. Therefore, we regress the translation from the input image directly in the second stage.

We make use of the idea of anchors introduced in [32] to formulate pose estimation as hybrid classification/regression problem. Specifically, we derive the continuous 3 DoF rotation from the pose embedding vector by classifying the rotation into a specific discrete rotation anchor and regressing the residual between the anchor and the actual rotation. Selecting the parameterization is essential for rotation estimation. Ideally, our *anchors* should divide the rotation space $\mathcal{SO}(3)$ into bins of the same size. Therefore, we make use of the uniform quaternion sampling method described in [38]. Specifically, by sampling $u_1, u_2, u_3 \in [0, 1]$, a quaternion anchor can be obtained by:

$$\mathbf{q} = (\sqrt{1 - u_1} \sin 2\pi u_2, \sqrt{1 - u_1} \cos 2\pi u_2, \sqrt{u_1} \sin 2\pi u_3, \sqrt{u_1} \cos 2\pi u_3). \quad (1)$$

We thus obtain our anchors by uniformly gridding each dimension with N values, resulting in $N \times N \times N$ quaternion anchors¹. The residual \mathbf{q}_d between anchor quaternion \mathbf{q}_a and the ground truth \mathbf{q}_{gt} can be obtained with

$$\mathbf{q}_d = \mathbf{q}_{gt} \mathbf{q}_a^{-1} \quad (2)$$

The ground truth anchor class label is found by comparing the ground truth rotation to all anchors using the geodesic distance:

$$d(\mathbf{q}_{gt}, \mathbf{q}_a) = 2\cos^{-1}(|\langle \mathbf{q}_{gt}, \mathbf{q}_a \rangle|). \quad (3)$$

Note that, to enforce the constraint $\|\mathbf{q}\| = 1$, we use L2 normalization as activation function for the last layer of rotation residual regression sub-network. We use a cross entropy loss as the anchor classification loss and the Huber loss as the residual regression loss.

3.3. 3D Shape Retrieval and Pose Estimation from Images (Stage II)

In the second stage of our method, we retrieve the 3D shape and estimate the 6D pose of the object. As shown in Figure 2 **Stage II**, we train a ResNet [18] to map the image to the ground truth embedding vectors with the L1 loss. The ground truth embedding vectors are obtained by applying the *embedding network* on the 3D volume of the ground truth shape in the ground truth rotation. In addition, similarly to the *embedding network*, the *regression network* contains a sub-network for shape classification trained with a cross-entropy loss and another sub-network for the rotation regression trained with an *anchor+residual* loss.

The absolute 3D translation of the object cannot be obtained without knowing the camera intrinsic parameters, the image cropping and the dimension of the object. However, in order to be able to overlay the object onto the image, we estimate the up-to-scale 3D translation with respect to the image cropped with the object bounding box, assuming a common camera model and normalized 3D shape. The regression of 3D translation is performed similarly as the rotation regression with a sub-network trained using another *anchor+residual* loss. To this end, the translation anchors are obtained by dividing the Euclidean space into equal cubes centered at \mathbf{t}_a . During training, we normalize the residual translation \mathbf{t}_d using the dimension of the corresponding anchor cube to constrain it within range $[0, 1]$. We use cross entropy loss for the anchor cube classification and Huber loss for regressing the translation residual regression within the anchor cube.

During testing, we only feed a single image into the *regression network* and obtain the shape label to retrieve the closest 3D model from the database as well as the 6D pose.

¹ $N = 7$ in all our experiments. The method of [38] can yield duplicated anchors. However, they are removed during training by our closest anchor search, which leads to 259 unique anchors.

3.4. Implementation Details

For training the *embedding network* in Stage I, we use a similar architecture as *VoxNet* [28]. The dimensionality of the embedding vectors for both shape and pose is 512. For our *regression network* in Stage II, we use the ResNet50 [18] pre-trained on ImageNet [11] as the backbone network. The *embedding network* is pre-trained with the aligned version [36] of ModelNet40 subset of ShapeNet dataset [8]. Our networks are trained with Adam optimizer with a learning rate of 10^{-4} . We train the *embedding network* for 100 epochs and we generate 10,000 samples during each epoch. Our *regression network* is trained for 16 epochs.

We use PyTorch library for all our implementations. Our training scheme for the *embedding network* relies on generating input 3D data in random poses in an online manner, and therefore we also need to generate the ground truth pose anchor label for each input instance. To make this nearest neighbour search more efficient, we make use of a KD-tree implementation.

For training the *regression network*, the range of the translation vector is restricted to $x \in [-0.25, 1.5]$, $y \in [-0.25, 1.5]$ and $z \in [0.5, 10.0]$, which is determined by the translation range in the training data.

4. Experiments

To demonstrate the effectiveness of our approach, we conduct experiments on the benchmark dataset Pascal3D+ [48]. We first provide the qualitative results and quantitative comparisons with the state-of-the-art methods for both 3D shape retrieval and pose estimation tasks. Then, we evaluate the importance of each main component of our approach. Finally, we perform an error analysis to discuss the failure cases.

4.1. Dataset

We perform our experiments on the Pascal3D+ dataset [48]. In this dataset, there are 13,898 object instances that appear in 8,505 images from PASCAL VOC images. Additionally, 22,394 images from ImageNet are annotated. For every instances, pose of the 3D object which aligned with the images are annotated. There are 12 general categories and 79 unique models. The general categories are *aeroplane, bicycle, boat, bottle, bus, car, chair, dining table, motorbike, sofa, train, and tv monitor*. On average there are more than 3,000 instances per category.

4.2. Comparison to the State-of-the-Art

Following many existing methods [16, 40, 43], we use the images cropped with the ground truth object bounding boxes as input to our method. To evaluate our method qualitatively, we render the retrieved 3D CAD model in the es-

timated pose. These qualitative results with comparison to the ground truth are shown in Figure. 3, where one example is shown for each category. In the following, we provide the quantitative comparisons on 3D pose estimation and 3D shape retrieval tasks.

4.2.1 3D Pose Estimation

For 3D pose estimation task, We provide the quantitative comparisons against the existing methods on two metrics *MedErr* and $Acc_{\frac{\pi}{6}}$. *MedErr* is a robust measure of pose prediction accuracy by considering the median of pose errors on all instances quantified as the geodesic distance between ground truth rotation and the predicted rotation. As we parametrize our rotation using quaternions, geodesic distance between two quaternions can be obtained using Eq. 3. This is equivalent to the following rotation matrix based formulation used in most of the related works:

$$d(R_1, R_2) = \frac{\|\log(R_1 R_2^T)\|_F}{\sqrt{2}}. \quad (4)$$

$Acc_{\frac{\pi}{6}}$ is the percentage of the instances, for which the pose errors are smaller than 30° . Following the standard evaluation protocol, we exclude truncated and occluded objects from the test dataset.

Our results are shown in Table. 1. Note that all the compared methods except for [16] are category-specific. Their pose prediction network is composed of a collection of networks tailored for each category. For Pascal3D+, there will be 12 pose prediction networks for each 12 category. The reason for this is to exploit the biases in view point angle in the training data for a specific category. In contrast, our pose estimation is category-agnostic by using a single sub-network for all categories, which is more scalable to datasets with a large amount of object categories. Therefore, our disentangled embedding significantly improves the pose estimation performance over a shared embedding for pose and shape. In addition, their reported numbers are achieved by using ground truth category labels to select the specific pose networks, which is impractical in real world scenarios. Therefore, for fair comparisons, we split Table. 1 to two groups. We can see that, our approach significantly outperforms the state-of-the-art method of [16] in the category-agnostic setting. Moreover, our method even outperforms all the category-specific methods in both *MedErr* and $Acc_{\frac{\pi}{6}}$ metrics, although we do not use any ground truth labels.

4.2.2 3D Shape Retrieval

We evaluate 3D shape retrieval performance of our approach using the Top-1-Acc metric and compare against [16], which reported the state-of-the-art 3D shape

Table 1. Pose estimation comparison on Pascal3D+. Best results are highlighted in bold. We do not differentiate between category-specific and category-agnostic when considering the best results.

	category-specific												Mean
	aero	bike	boat	bottle	bus	car	chair	dtable	mbike	sofa	train	tv	
\downarrow MedErr ([43])	13.8	17.7	21.3	12.9	5.8	9.1	14.8	15.2	14.7	13.7	8.7	15.4	13.59
\downarrow MedErr ([30])	13.6	12.5	22.8	8.3	3.1	5.8	11.9	12.5	12.3	12.8	6.3	11.9	11.1
\downarrow MedErr ([40])	15.4	14.8	25.6	9.3	3.6	6.0	9.7	10.8	16.7	9.5	6.1	12.6	11.7
\downarrow MedErr ([16])	10.0	15.6	19.1	8.6	3.3	5.1	13.7	11.8	12.2	13.5	6.7	11.0	10.9
\uparrow Acc $\frac{\pi}{6}$ ([43])	0.81	0.77	0.59	0.93	0.98	0.89	0.80	0.62	0.88	0.82	0.80	0.80	0.8075
\uparrow Acc $\frac{\pi}{6}$ ([30])	0.78	0.83	0.57	0.93	0.94	0.90	0.80	0.68	0.86	0.82	0.82	0.85	0.8103
\uparrow Acc $\frac{\pi}{6}$ ([40])	0.74	0.83	0.52	0.91	0.91	0.88	0.86	0.73	0.78	0.90	0.86	0.92	0.8200
\uparrow Acc $\frac{\pi}{6}$ ([16])	0.83	0.82	0.64	0.95	0.97	0.94	0.80	0.71	0.88	0.87	0.80	0.86	0.8392
	category-agnostic												Mean
	aero	bike	boat	bottle	bus	car	chair	dtable	mbike	sofa	train	tv	
\downarrow MedErr ([16])	10.9	12.2	23.4	9.3	3.4	5.2	15.9	16.2	12.2	11.6	6.3	11.2	11.5
\downarrow MedErr (Ours)	10.1	14.0	25.7	9.4	3.8	7.6	14.4	17.2	16.9	12.9	8.1	10.8	10.8
\uparrow Acc $\frac{\pi}{6}$ ([16])	0.80	0.82	0.57	0.90	0.97	0.94	0.72	0.67	0.90	0.80	0.82	0.85	0.8133
\uparrow Acc $\frac{\pi}{6}$ (Ours)	0.85	0.82	0.58	0.96	0.97	0.93	0.87	0.76	0.77	0.75	0.79	0.87	0.851

Table 2. 3D model retrieval accuracy using ground truth detections on Pascal3D+ in terms of Top-1-Acc.

Method	aero	bike	boat	bottle	bus	car	chair	table	mbike	sofa	train	tv	mean
[16]	0.48	0.31	0.60	0.41	0.78	0.41	0.29	0.19	0.43	0.36	0.65	0.61	0.460
Ours w/o embedding	0.53	0.52	0.69	0.48	0.62	0.45	0.24	0.37	0.58	0.32	0.53	0.59	0.456
Ours w/o disentangling	0.57	0.49	0.66	0.49	0.65	0.47	0.26	0.43	0.59	0.20	0.56	0.58	0.463
Ours	0.59	0.57	0.73	0.53	0.66	0.52	0.32	0.46	0.63	0.40	0.57	0.62	0.514

retrieval results on Pascal3D+ dataset. This task is challenging because some models in Pascal3D+ are quite similar to each other. In addition, majority of the object instances do not have an exact 3D model. For some of the images, it is unclear which model should be the correct ground truth.

The results for 3D shape retrieval are given in Table 2. Our approach achieved an mean Top-1-Acc of 0.514, which outperforms the state-of-the-art method of [16] (0.460) by a large margin. A disadvantage of their method is that its retrieval performance depends on not only the retrieval method, but also the pose estimation, since their retrieval is based on depth images rendered with the estimated pose. Therefore, an error in pose estimation will drastically exaggerate the errors in shape retrieval. In contrast, our approach explicitly disentangles the shape and pose embedding, and thus each embedding representation is invariant to the other. Note that our accuracy is even higher than the highest accuracy reported in [16] (0.4967), which is achieved by using the ground truth poses, and thus can be considered to be the theoretical upper bound of their method.

4.3. Ablation Study

To understand the behaviour of our method and the effect of each feature of our approach, we perform ablation experiments and present the results in Table 2 and Table 3.

In order to evaluate the importance of the disentangled embedding learning, we conduct experiments with two

baseline methods: 1) **Ours w/o embedding**, where we only train the *regression network* purely on image input in a single stage pipeline. 2) **Ours w/o disentangling**, where instead of having two separate embedding vectors of dimension 512 for both pose and shape, we use a single embedding vector of dimension 1024. In the following, we discuss the results of these experiments for both shape retrieval and pose estimation tasks.

4.3.1 3D Shape Retrieval

From Table 2, comparing **Ours w/o embedding** against **Ours w/o disentangling**, we can see that learning an embedding from pure 3D data is helpful for the retrieval task. However, this improvement is incremental. In contrast, if we remove the pose information from the embedding with our disentangling of shape and pose, the retrieval performance is boosted by a large margin (**Ours w/o disentangling** vs. **Ours**). This indicates that the pose variation is also distracting for the 3D shape retrieval, which has to be removed for better performance.

4.3.2 3D Pose Estimation

From Table 3, we can see that our disentangled embedding learning is also moderately helpful for the pose estimation task (**Ours w/o embedding** vs. **Ours**). We notice here the

discrepancy between the evaluation metrics of *MedErr* and $Acc_{\frac{\pi}{6}}$ – that is, it improves in $Acc_{\frac{\pi}{6}}$ but degrades in *MedErr*. We believe that this discrepancy is due to the characteristic of the *MedErr* metric. Although *MedErr* is robust against outliers, it is over sensitive to fluctuations, as it is concerned with only one sample, i.e. the middle sample. Therefore, when two algorithms yield very similar *MedErr*, one should weigh more on the $Acc_{\frac{\pi}{6}}$ metric, which takes into account all available samples and is more indicative of the overall performance of the algorithms.

When comparing **Ours w/o embedding** against **Ours w/o disentangling**, we can see that the pose estimation performance degrades significantly if we use a common embedding for shape and pose to guide our *regression network*. Our interpretation of this is as follows: The random poses applied on the 3D data is sampled from a uniform distribution. However, the pose distribution for specific category is highly biased. Therefore, if we do not disentangle the pose and shape to make the pose invariant to the categories, the distribution of our 3D training data does not resemble the distribution of the image data. In contrast, the distribution of the category-independent pose embedding is closer to a uniform distribution.

Number of anchors. We also study the effect of different number of anchors on pose estimation task and present results in Table. 3. Using one anchor is equivalent to direct regression and our result is comparable to the results presented in [25], which also performs direct regression. The poor results are consistent with other findings in the literature [42] where regression performs consistently worse than classification for pose estimation. However, with just a small number of anchors (4^3), the pose estimation accuracy rapidly increases. We found the optimal configuration of 7^3 anchors and no performance advantage can be obtained beyond this point. Although 9^3 anchors more densely sample the rotation space, we speculate that as the number of parameters grows exponentially, optimization difficulty comes into play for both anchor classification and residual regression networks.

Table 3. Ablation study on pose estimation performance.

Method	$\downarrow MedErr$	$\uparrow Acc_{\frac{\pi}{6}}$
Grabner et. al.[16]	11.5	0.8133
Ours w/o embedding (1^3 anchors)	17.1	0.74
Ours w/o embedding (4^3 anchors)	11.1	0.81
Ours w/o embedding (7^3 anchors)	10.6	0.843
Ours w/o embedding (9^3 anchors)	11.2	0.831
Ours w/o disentangling (7^3 anchors)	13.2	0.77
Ours (7^3 anchors)	10.8	0.851

Table 4. Error analysis based on object characteristics.

Retrieval		
Setting	Top-1-Acc	
Default	0.514	
Small Objects	0.485	
Large Objects	0.552	
Occluded Objects	0.457	
Truncated Objects	0.443	
Pose		
Setting	$\downarrow MedErr$	$\uparrow Acc_{\frac{\pi}{6}}$
Default	10.6	0.851
Small Objects	11.36	0.81
Large Objects	10.66	0.879
Occluded Objects	15.49	0.78
Truncated Objects	18.34	0.75

4.4. Error Analysis

We now provide detailed analysis of our failure cases. Both shape retrieval and pose estimation tasks share some of the common causes: 1) blurry or small object instances, 2) ambiguity of the ground truth label and 3) truncated or occluded objects. We provide an analysis of our failure modes in terms of object characteristics in Table. 4. We define 'Large Objects' as the top one third of instances sorted by bounding box size and 'Small Objects' the bottom one third. We also show the results for truncated and occluded objects for pose estimation task even though they are excluded from evaluation shown in Table. 1. We can see that the method performs worse on small, occluded or truncated objects.

Category specific failure modes are significantly different for shape retrieval and pose estimation. For retrieval, we yield lowest accuracy on chair and sofa. We attribute this mainly to large intra-class variation among object instances in the images and the fact that one can not find the exact or sufficiently similar 3D objects from the database. We also note that there are several errors in the annotation. An example can be seen in Figure. 5 (2nd row left) where the jet fighter is incorrectly labelled as passenger airplane, whereas we retrieve the correct shape.

For pose estimation, the boat score is significantly lower than other categories. There are large intra-class differences for boat category for both object instances in the image and the 3D models. Only one of the 3D models of boats has sails, which are unfurled. However, in many cases the sails of the boats in the images are furled. There is also significant ambiguity in many instances of boats where it is unclear which part of the boat is front and back. In such cases, we typically fail by predicting a different front and back pose than the ground truth annotation. Other causes of error are similar to retrieval, where blurry images and incorrect annotation lead to errors. Failure cases for pose estimation are shown in Figure. 4. An ambiguous example is the

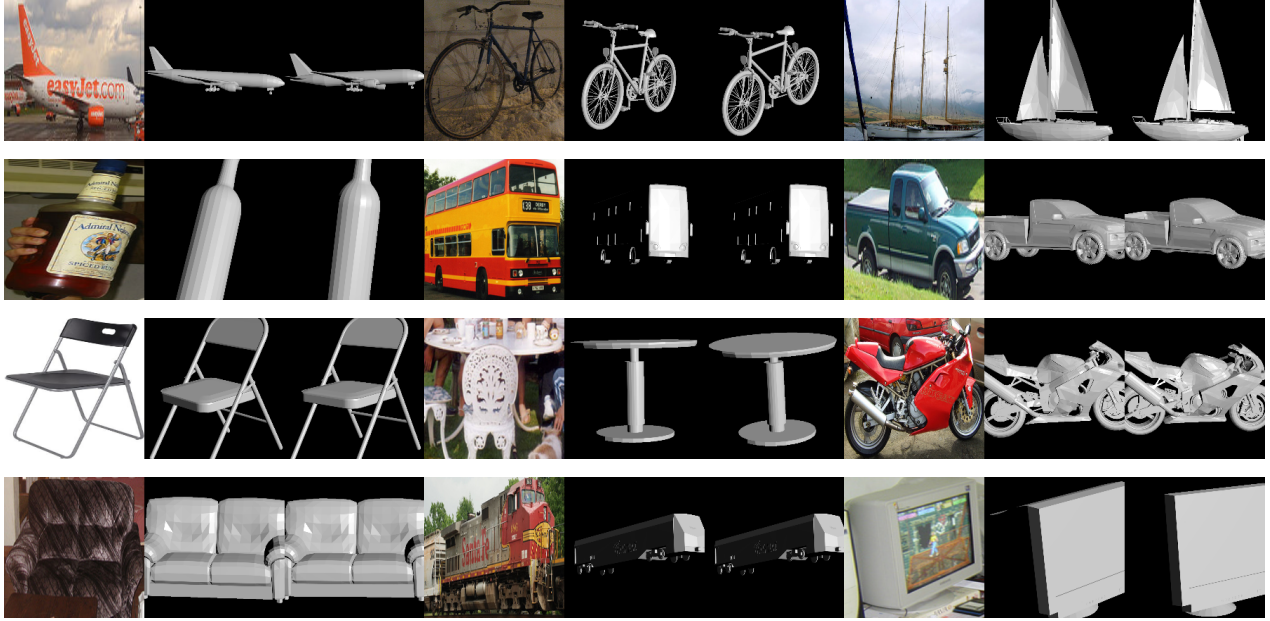


Figure 3. Qualitative results for pose estimation and 3d model retrieval on Pascal3D+ dataset. We show example results for all 12 categories. For each instance, the first column is the original image, the second column is image rendered using ground truth pose and model and the last column is rendered our predicted pose and model.

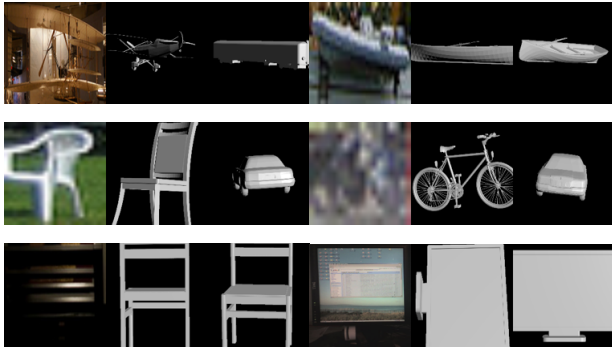


Figure 4. Example failure cases for pose estimation task. We render the figures using predicted pose and 3D shape. Therefore, it maybe possible that both pose and retrieval are wrong in the examples. However, all the examples here have incorrect pose.

monitor shown in Figure. 4 (3rd row right). Even though the monitor is rotated 90° , the stand is still in the original configuration. This violates our assumption that the objects are rigid. It is interesting to explore in the future how to address the pose estimation for such articulated objects.

5. Conclusion

Joint 3D shape retrieval and pose estimation from monocular images is an important and challenging task that has a wide range of applications in robotics and augmented reality applications. To factor out the distracting factors in the images, we learn an embedding space explicitly disen-

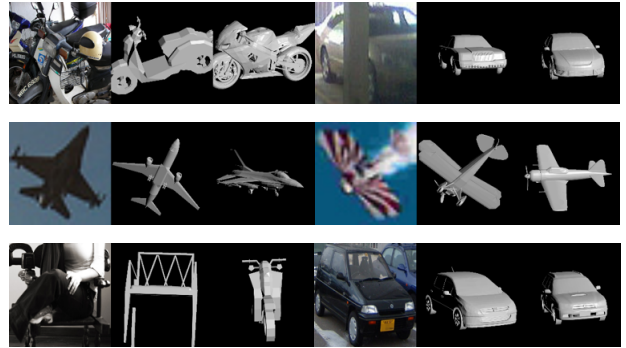


Figure 5. Example failure cases for 3D model retrieval task. Note that unlike pose estimation task, we include both occluded and truncated objects in the evaluation. The top right car failure is caused by truncation and the bottom right chair failure is caused by occlusion.

tangled for shape and pose from pure 3D data, which is free from distracting factors in the images. Our disentangled representation allows us to learn separated and more complete manifolds for pose and shape, which improves the generalization performance of our method on images of objects under unseen poses. Our proposed method outperforms the previous state-of-the-art methods on both shape retrieval and pose estimation tasks on the challenging Pascal3D+ dataset. Future work can be alternating the representation of 3D models for better discriminativity. We are also motivated to explore further in the same direction

where we map real world images to useful and task specific representation spaces.

6. Acknowledgement

This research is part of NExT research which is supported by the National Research Foundation, Prime Ministers Office, Singapore under its IRC@SG Funding Initiative. It is partially supported by German Research Foundation (DFG CRC 1223).

References

- [1] Z. Akata, F. Perronnin, Z. Harchaoui, and C. Schmid. Label-embedding for attribute-based classification. In *Proceedings of the IEEE Conference on Computer Vision and Pattern Recognition*, pages 819–826, 2013. 3
- [2] Z. Akata, S. Reed, D. Walter, H. Lee, and B. Schiele. Evaluation of output embeddings for fine-grained image classification. In *Proceedings of the IEEE Conference on Computer Vision and Pattern Recognition*, pages 2927–2936, 2015. 3
- [3] M. Aubry, D. Maturana, A. A. Efros, B. C. Russell, and J. Sivic. Seeing 3d chairs: exemplar part-based 2d-3d alignment using a large dataset of cad models. In *Proceedings of the IEEE conference on computer vision and pattern recognition*, pages 3762–3769, 2014. 1, 2
- [4] M. Aubry and B. C. Russell. Understanding deep features with computer-generated imagery. In *Proceedings of the IEEE International Conference on Computer Vision*, pages 2875–2883, 2015. 1, 2
- [5] S. Bai, X. Bai, Z. Zhou, Z. Zhang, and L. Jan Latecki. Gift: A real-time and scalable 3d shape search engine. In *Proceedings of the IEEE Conference on Computer Vision and Pattern Recognition*, pages 5023–5032, 2016. 2
- [6] S. Biasotti, A. Cerri, M. Aono, A. B. Hamza, V. Garro, A. Giachetti, D. Giorgi, A. Godil, C. Li, C. Sanada, et al. Retrieval and classification methods for textured 3d models: a comparative study. *The Visual Computer*, 32(2):217–241, 2016. 2
- [7] A. Brock, T. Lim, J. M. Ritchie, and N. Weston. Generative and discriminative voxel modeling with convolutional neural networks. *arXiv preprint arXiv:1608.04236*, 2016. 2
- [8] A. g. X. Chang, T. Funkhouser, L. Guibas, P. Hanrahan, Q. Huang, Z. Li, S. Savarese, M. Savva, S. Song, H. Su, et al. Shapenet: An information-rich 3d model repository. *arXiv preprint arXiv:1512.03012*, 2015. 5
- [9] K. Chen, C. B. Choy, M. Savva, A. X. Chang, T. Funkhouser, and S. Savarese. Text2shape: Generating shapes from natural language by learning joint embeddings. *arXiv preprint arXiv:1803.08495*, 2018. 3
- [10] G. Dai, J. Xie, and Y. Fang. Deep correlated holistic metric learning for sketch-based 3d shape retrieval. *IEEE Transactions on Image Processing*, 2018. 3
- [11] J. Deng, W. Dong, R. Socher, L.-J. Li, K. Li, and L. Fei-Fei. Imagenet: A large-scale hierarchical image database. In *Computer Vision and Pattern Recognition, 2009. CVPR 2009. IEEE Conference on*, pages 248–255. Ieee, 2009. 5
- [12] A. Frome, G. S. Corrado, J. Shlens, S. Bengio, J. Dean, T. Mikolov, et al. Devise: A deep visual-semantic embedding model. In *Advances in neural information processing systems*, pages 2121–2129, 2013. 3
- [13] R. Girdhar, D. F. Fouhey, M. Rodriguez, and A. Gupta. Learning a predictable and generative vector representation for objects. In *European Conference on Computer Vision*, pages 484–499. Springer, 2016. 2
- [14] Y. Goldberg and O. Levy. word2vec explained: deriving mikolov et al.’s negative-sampling word-embedding method. *arXiv preprint arXiv:1402.3722*, 2014. 2, 3
- [15] Y. Gong, Q. Ke, M. Isard, and S. Lazebnik. A multi-view embedding space for modeling internet images, tags, and their semantics. *International journal of computer vision*, 106(2):210–233, 2014. 3
- [16] A. Grabner, P. M. Roth, and V. Lepetit. 3d pose estimation and 3d model retrieval for objects in the wild. In *Proceedings of the IEEE Conference on Computer Vision and Pattern Recognition*, pages 3022–3031, 2018. 1, 2, 3, 5, 6, 7
- [17] R. A. Güler, G. Trigeorgis, E. Antonakos, P. Snape, S. Zafeiriou, and I. Kokkinos. Densereg: Fully convolutional dense shape regression in-the-wild. In *CVPR*, volume 2, page 5, 2017. 3
- [18] K. He, X. Zhang, S. Ren, and J. Sun. Deep residual learning for image recognition. In *Proceedings of the IEEE conference on computer vision and pattern recognition*, pages 770–778, 2016. 4, 5
- [19] H. Izadinia, Q. Shan, and S. M. Seitz. Im2cad. In *Computer Vision and Pattern Recognition (CVPR), 2017 IEEE Conference on*, pages 2422–2431. IEEE, 2017. 1, 2
- [20] A. Jourabloo and X. Liu. Large-pose face alignment via cnn-based dense 3d model fitting. In *The IEEE Conference on Computer Vision and Pattern Recognition (CVPR)*, June 2016. 3
- [21] A. Karpathy and L. Fei-Fei. Deep visual-semantic alignments for generating image descriptions. In *Proceedings of the IEEE conference on computer vision and pattern recognition*, pages 3128–3137, 2015. 3
- [22] A. Kumar, A. Alavi, and R. Chellappa. Kepler: Keypoint and pose estimation of unconstrained faces by learning efficient h-cnn regressors. In *Automatic Face & Gesture Recognition (FG 2017), 2017 12th IEEE International Conference on*, pages 258–265. IEEE, 2017. 3
- [23] C. Li, J. Bai, and G. D. Hager. A unified framework for multi-view multi-class object pose estimation. *arXiv preprint arXiv:1803.08103*, 2018. 3
- [24] Y. Li, H. Su, C. R. Qi, N. Fish, D. Cohen-Or, and L. J. Guibas. Joint embeddings of shapes and images via cnn image purification. *ACM Transactions on Graphics (TOG)*, 34(6):234, 2015. 2, 4
- [25] S. Mahendran, H. Ali, and R. Vidal. 3d pose regression using convolutional neural networks. In *IEEE International Conference on Computer Vision*, 2017. 3, 7
- [26] S. Mahendran, H. Ali, and R. Vidal. A mixed classification-regression framework for 3d pose estimation from 2d images. *arXiv preprint arXiv:1805.03225*, 2018. 3

- [27] F. Massa, B. C. Russell, and M. Aubry. Deep exemplar 2d-3d detection by adapting from real to rendered views. In *Proceedings of the IEEE Conference on Computer Vision and Pattern Recognition*, pages 6024–6033, 2016. 1
- [28] D. Maturana and S. Scherer. Voxnet: A 3d convolutional neural network for real-time object recognition. In *Intelligent Robots and Systems (IROS), 2015 IEEE/RSJ International Conference on*, pages 922–928. IEEE, 2015. 2, 4, 5
- [29] P. Min. binvox. <http://www.patrickmin.com/binvox> or <https://www.google.com/search?q=binvox>. 4
- [30] A. Mousavian, D. Anguelov, J. Flynn, and J. Košecká. 3d bounding box estimation using deep learning and geometry. In *Computer Vision and Pattern Recognition (CVPR), 2017 IEEE Conference on*, pages 5632–5640. IEEE, 2017. 6
- [31] J. Pennington, R. Socher, and C. Manning. Glove: Global vectors for word representation. In *Proceedings of the 2014 conference on empirical methods in natural language processing (EMNLP)*, pages 1532–1543, 2014. 3
- [32] S. Ren, K. He, R. Girshick, and J. Sun. Faster r-cnn: Towards real-time object detection with region proposal networks. In *Advances in neural information processing systems*, pages 91–99, 2015. 3, 4
- [33] G. Rogez, P. Weinzaepfel, and C. Schmid. Lcr-net: Localization-classification-regression for human pose. In *CVPR 2017-IEEE Conference on Computer Vision & Pattern Recognition*, 2017. 3
- [34] M. Savva, F. Yu, H. Su, M. Aono, B. Chen, D. Cohen-Or, W. Deng, H. Su, S. Bai, X. Bai, et al. Shrec16 track large-scale 3d shape retrieval from shapenet core55. In *Proceedings of the eurographics workshop on 3D object retrieval*, 2016. 2
- [35] F. Schroff, D. Kalenichenko, and J. Philbin. Facenet: A unified embedding for face recognition and clustering. In *Proceedings of the IEEE conference on computer vision and pattern recognition*, pages 815–823, 2015. 4
- [36] N. Sedaghat, M. Zolfaghari, E. Amiri, and T. Brox. Orientation-boosted voxel nets for 3d object recognition. *arXiv preprint arXiv:1604.03351*, 2016. 2, 5
- [37] B. Shi, S. Bai, Z. Zhou, and X. Bai. Deeppano: Deep panoramic representation for 3-d shape recognition. *IEEE Signal Processing Letters*, 22(12):2339–2343, 2015. 2
- [38] K. Shoemake. *Graphics Gems III*. Academic Press Professional, Inc., San Diego, CA, USA, 1992. 4
- [39] H. Su, S. Maji, E. Kalogerakis, and E. Learned-Miller. Multi-view convolutional neural networks for 3d shape recognition. In *Proceedings of the IEEE international conference on computer vision*, pages 945–953, 2015. 2
- [40] H. Su, C. R. Qi, Y. Li, and L. J. Guibas. Render for cnn: Viewpoint estimation in images using cnns trained with rendered 3d model views. In *Proceedings of the IEEE International Conference on Computer Vision*, pages 2686–2694, 2015. 3, 5, 6
- [41] F. P. Tasse and N. Dodgson. Shape2vec: semantic-based descriptors for 3d shapes, sketches and images. *ACM Transactions on Graphics (TOG)*, 35(6):208, 2016. 2, 3
- [42] S. Tulsiani, S. Gupta, D. Fouhey, A. A. Efros, and J. Malik. Factoring shape, pose, and layout from the 2d image of a 3d scene. In *Computer Vision and Pattern Recognition (CVPR)*, 2018. 7
- [43] S. Tulsiani and J. Malik. Viewpoints and keypoints. In *Proceedings of the IEEE Conference on Computer Vision and Pattern Recognition*, pages 1510–1519, 2015. 3, 5, 6
- [44] Z. Wu, S. Song, A. Khosla, F. Yu, L. Zhang, X. Tang, and J. Xiao. 3d shapenets: A deep representation for volumetric shapes. In *The IEEE Conference on Computer Vision and Pattern Recognition (CVPR)*, June 2015. 2
- [45] Z. Wu, Y. Zhang, M. Zeng, F. Qin, and Y. Wang. Joint analysis of shapes and images via deep domain adaptation. *Computers & Graphics*, 70:140–147, 2018. 3
- [46] Y. Xian, Z. Akata, G. Sharma, Q. Nguyen, M. Hein, and B. Schiele. Latent embeddings for zero-shot classification. In *Proceedings of the IEEE Conference on Computer Vision and Pattern Recognition*, pages 69–77, 2016. 3
- [47] Y. Xiang, W. Kim, W. Chen, J. Ji, C. Choy, H. Su, R. Mottaghi, L. Guibas, and S. Savarese. Objectnet3d: A large scale database for 3d object recognition. In *European Conference Computer Vision (ECCV)*, 2016. 1, 2, 4
- [48] Y. Xiang, R. Mottaghi, and S. Savarese. Beyond pascal: A benchmark for 3d object detection in the wild. In *Applications of Computer Vision (WACV), 2014 IEEE Winter Conference on*, pages 75–82. IEEE, 2014. 2, 4, 5
- [49] X. Zhu, Z. Lei, X. Liu, H. Shi, and S. Z. Li. Face alignment across large poses: A 3d solution. In *Proceedings of the IEEE conference on computer vision and pattern recognition*, pages 146–155, 2016. 3
- [50] Z. Zhu, X. Wang, S. Bai, C. Yao, and X. Bai. Deep learning representation using autoencoder for 3d shape retrieval. *Neurocomputing*, 204:41–50, 2016. 2